

Metrology for quality control and alignment of CAT grating spectrometers

Jungki Song,¹ Ralf K. Heilmann,¹ Alexander R. Bruccoleri,²
Edward Hertz,³ and Mark L. Schattenburg¹

¹Space Nanotechnology Laboratory, MIT Kavli Institute for Astrophysics and Space Research,
Massachusetts Institute of Technology, Cambridge, Massachusetts 02139, USA

²Izentis LLC, PO Box 397002, Cambridge, MA 02139, USA

³Harvard-Smithsonian Center for Astrophysics, Cambridge, MA 02138, USA

ABSTRACT

Arcus, a mission proposed as a Medium Size Explorer for high-resolution x-ray spectroscopy, requires unprecedented sensitivities: high resolving power ($\lambda/\Delta\lambda > 2500$) and large collecting area ($\sim 350 \text{ cm}^2$). The core instruments on Arcus are Critical-Angle Transmission (CAT) grating spectrometers consisting of hundreds of co-aligned diffraction gratings. The gratings require thorough quality control along the entire manufacturing process: from bare silicon wafers to CAT grating petal assembly. Period variation, grating bar tilt angles, misalignment, and grating film buckling are potential errors of interest which could degrade the performance of the x-ray grating spectrometer. We present progress towards development of metrology techniques to measure and manage aforementioned errors during the entire alignment and integration processes: starting right after fabrication of CAT grating membranes to their assembly into large arrays. A scanning laser reflection tool (SLRT) was developed to measure period variations, alignment, and area percentage of pinched grating bars. An array of four CAT gratings was successfully aligned to satisfy Arcus alignment allocations for a grating window alignment test (GWAT). No discernible signal was found from an effort to measure a 'half' diffraction order to characterize stiction between grating bars. A metrology protocol was developed to measure grating bar tilt angle variations and average bar tilt angles relative to the grating surface normal, based on small-angle x-ray scattering (SAXS, Cu-K α) and an optical surface normal measurement (OSNM) setup. A grating holder was designed with integrated slits to relate independent measurements from two different setups using visible and x-ray beams. Bar tilt variations of 1 degree and average bar tilt angles of ~ 0.3 degree were observed for seven different CAT grating samples. Bar tilt angle variations induced from buckled grating films were also measured. We discuss implications for a more demanding CAT grating spectrometer for the proposed Lynx X-ray Surveyor mission to be presented to the next Astrophysics Decadal Survey.

1. INTRODUCTION

Arcus is a Medium Size Explorer proposed for high-resolution soft x-ray spectroscopy and selected for a Phase A concept study, demanding unprecedented resolving power ($\lambda/\Delta\lambda > 2500$) and large collecting area ($\sim 350 \text{ cm}^2$) to meet its challenging science requirements [1,2]. It features four parallel optical channels, each consisting of a critical-angle transmission (CAT) grating petal co-aligned with a petal holding an array of 34 confocal silicon pore optic (SPO) mirror modules based on the Athena design [3]. Each CAT grating petal is populated with 176 co-aligned CAT gratings, distributed over 34 grating windows that hold four or six gratings each (total of 704 CAT gratings) [1, 2].

A CAT grating is a blazed transmission grating which has several advantages compared to reflection gratings, including relaxed alignment and surface flatness tolerances and low mass-to-area ratio [4-7]. Until recently, transmission gratings have been rarely proposed for soft x-ray grating spectrometer missions ever since high energy transmission gratings (HETGs) [8] were deployed into space onboard the *Chandra X-ray Observatory* with its unparalleled 0.5 arcsec angular point spread function (PSF). To overcome the much higher “blur” of thin-foil x-ray mirror arrays employed for x-ray missions that require higher effective area than *Chandra*, the technology to blaze into high diffraction orders in transmission was lacking, and heavier, alignment-sensitive reflection gratings were the only option. However, recent advances in high resolution thin-shell x-ray mirrors [3] and CAT grating fabrication technology [9-15] have enabled a transmission grating spectrometer for high-resolution x-ray spectroscopy. Through continuous fabrication advances throughout the last decade, CAT grating technology has matured [9-15] such that reasonable numbers of 200 nm-period gratings can be produced with consistent quality to start developing metrology for quality control, assembly, and alignment.

Following William Thomson (Lord Kelvin), “*I often say that when you can measure what you are speaking about, and express it in numbers, you know something about it...*” [16], we list the following potential CAT grating imperfections that need to be measured to achieve Arcus performance requirements: period variations, grating bar tilt angle, misalignment, “pinched” grating bars stuck together from stiction, and grating film buckling (see Fig. 1). Period variation reduces resolving power by broadening diffraction peaks [17, 18] while bar tilt variations, misalignments, film buckling, and pinched bars are expected to adversely affect effective area [19, 20].

In the era of the *Chandra X-ray Observatory*, a laser reflection (LR) tool was developed for measurement of period variations [17], and roll alignment was performed based on the polarization properties of the gratings [21]. Although abandoned during the development process of HETGs, an attempt to measure bar tilt angle variation of the HETG fabricated using x-ray lithography based on scalar diffraction theory was found [22].

We report progress on the development of a scanning laser reflection tool (SLRT) for the Arcus CAT grating spectrometers [23]. The SLRT is designed to rapidly and precisely measure grating imperfections in air during the production of large arrays of gratings, eliminating the need for time-consuming x-ray characterization under vacuum. Its potential capability for alignment of gratings was also demonstrated. An array of four CAT gratings was aligned in-plane using the SLRT to satisfy Arcus tolerance allocations for a grating window alignment test (GWAT). It is expected to replace a polarization-based grating alignment tool used for the membrane-supported gold bar gratings on *Chandra*, which has the potential to suffer from metrology errors such as parasitic partial polarization from the integrated cross-support mesh (“L1 support mesh”) and stress birefringence from the silicon dioxide layers that are unique to our CAT grating

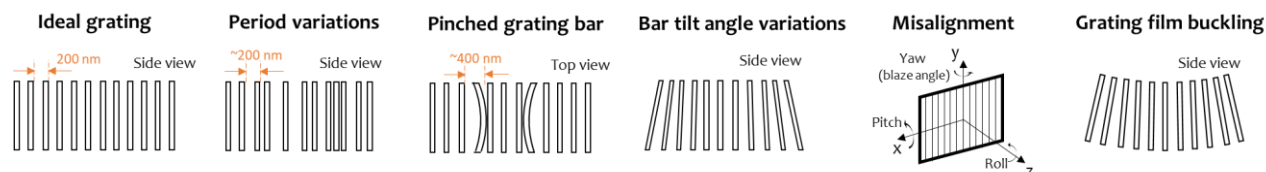


Figure 1. A schematic for an ideal CAT grating and potential CAT grating imperfections. Note that pinched grating bars and misalignment are shown in top and inclined views, respectively, while others are shown in side or cross-sectional view, with x rays incident from the top.

design. Its capability to measure grating film buckling and period variation for CAT gratings is still under development and will not be covered in this paper.

While most of the CAT grating imperfections can be measured with the SLRT, measurement of grating bar tilt angle variation requires a measurement technique based on x-ray wavelengths due to the very fine features of the grating bars. A small-angle x-ray scattering (SAXS, Cu-K α radiation) technique was employed, along with rigorous coupled-wave analysis (RCWA) to predict diffraction efficiencies as a function of rotation angle, to find bar tilt angles (details are shown in section 6). Unlike scalar diffraction theory, RCWA does not show any unphysical discontinuities when predicting diffraction efficiency as a function of tilt angle [24] and has been used successfully to characterize CAT grating diffraction efficiency. As SAXS alone cannot find the grating surface normal, an independent metrology setup and a custom grating holder that has a slit reference axis was developed (details are shown in section 6). This method of characterizing bar tilt angle distributions is important to optimize CAT grating alignment for Arcus.

Lynx, the mission concept studied for the next Decadal survey, requires a grating spectrograph with more demanding resolving power ($\lambda/\Delta\lambda > 5000$) and effective area ($> 4000 \text{ cm}^2$) [7] assuming Chandra-like mirror PSF, while providing 2 m^2 mirror effective area at a photon energy of 1 keV. These demanding goals will require further improvement in our grating metrology.

Sources of CAT grating imperfections are discussed in the following sections. We then describe a system configuration for the SLRT, followed by the results for the GWAT. We comment briefly on the attempted measurement of pinched grating bars using the SLRT. Finally, measurement and simulation results for grating bar tilt angles are shown based on SAXS with a newly developed measurement protocol.

2. SOURCES OF GRATING IMPERFECTION

Small systematic period variations due to spherical wave interference are intrinsic to the grating patterning technique used in this work [25, 26]. Measurement of this period distortion was reported in a previous paper [23]. CAT gratings consist of 200 nm-period freestanding ultra-high aspect ratio silicon grating bars, held in place by an integrated 5 μm -period cross-support mesh. We achieve this geometry using deep reactive-ion etching (DRIE) of a 4 μm thick $\langle 110 \rangle$ silicon-on-insulator (SOI) device layer, followed by a short, crystal-lattice-orientation dependent KOH wet etch. Details of the fabrication process can be found in Refs. 9-15. Non-vertical etching, leading to non-normal bar tilt angles, can be induced by an edge-low ion density profile which results in a non-uniform plasma sheath during the DRIE process [27, 28]. Misalignment between crystallographic orientation and the wafer surface normal could potentially be another source of angled grating bar sidewalls after KOH etching. A mechanism for grating film buckling has not yet been conclusively established, but is probably related to stress in the buried oxide layer. Its effect on bar tilt angle variations will also be discussed in Section 6.

3. SCANNING LASER REFLECTION TOOL (SLRT)

Figures 2a and 2b show a schematic and photograph of the SLRT developed for the measurement of period variation, grating film buckling, misalignments, and pinched grating bars. The system employs a 325 nm HeCd laser source, a high-precision XY stage, a 3-axis rotation stage, a grating holder, two 10 \times telescopes, three position-sensitive detectors (PSDs), and imaging optics. A vertical breadboard (see Fig. 2b) is supported by two 45-degree aluminum supports from the back to suppress mechanical vibrations. The beam from the UV laser is split into two beams, which are reflected by mirrors (or beam splitter) to be incident upon the same position on the grating with different incidence angles (55° and 0° for the angled-incidence and normal-incidence beams, respectively). 10 \times telescopes reduce the laser beam diameter to 150 μm on the grating surface for both angled and normal incidence beams (The angled beam is partially masked so that the projected beam forms a roughly circular shape on the grating surface.) Imaging optics capture light scattered from the grating surface

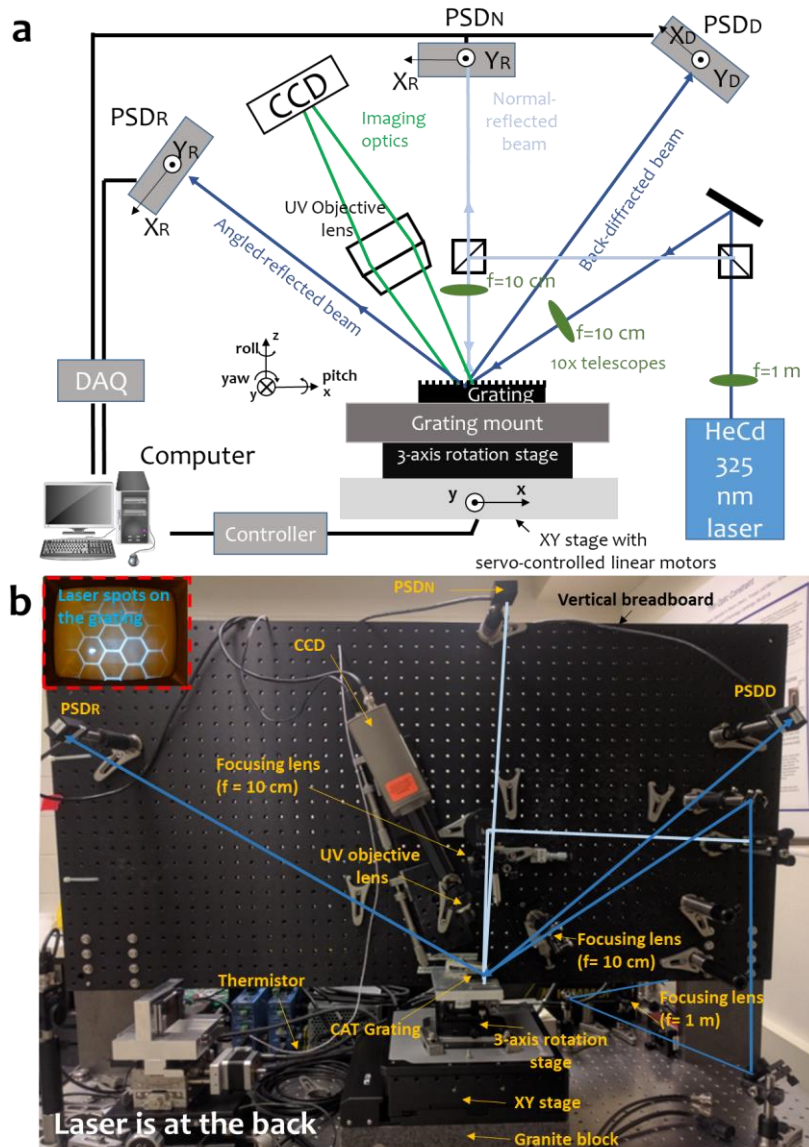


Figure 2. Scanning laser reflection tool (SLRT) developed for CAT grating metrology. (a) Schematic of the SLRT. (b) A photograph of the SLRT. Details on angles and beam path lengths are shown in our previous paper [23]. (Inset, upper left) Photograph of two incident beams (one normal and one at 55 degrees) located on the same position on the grating surface.

to locate the position of incident beams. The inset in the upper left corner in Figure 2b shows two incident beams located on the same position on the grating surface.

The SLRT works very well on flat gratings. However, the metrology becomes more challenging for non-flat gratings. A CAT grating film is basically a perforated 4- μm thin membrane that contains $\sim 1 \mu\text{m}$ wide, 5 μm -period L1 supports sitting on a buried oxide layer that connects the membrane to a 0.5 mm-thick, $\sim 1 \text{ mm}$ -period hexagonal silicon mesh. The 4 μm -tall CAT grating bars are suspended between the L1 supports. We observe that the grating film is sometimes buckled within a hexagon, with amplitudes ranging from $\sim 200 \text{ nm}$ up to a few microns. This non-flatness is probably induced by stress from left-over oxide etch masks or the left-over SOI buried oxide layer. The small amount of

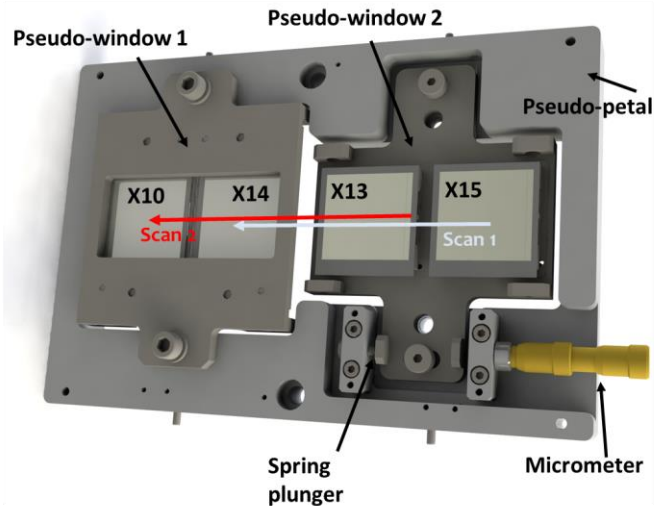


Figure 3. A schematic of the hardware used for GWAT alignment for Arcus.

buckling is not expected to impact grating resolving power for x-ray diffraction, but it can distort the profiles of reflected and diffracted UV laser beams, which can lead to unwanted shifts in the recorded PSD positions.

4. GRATING WINDOW ALIGNMENT TEST (GWAT)

The principle of alignment for the grating window alignment test (GWAT) is the same as described in our previous paper [23]. The array of four gratings was aligned in-plane on a pseudo-petal to satisfy the Arcus alignment allocation [18, 19] for the GWAT (see Fig. 3) (only two gratings were aligned in our previous paper [23]). After alignment, the petal was sent to the PANTER x-ray test facility in Germany for x-ray verification, and flown back to MIT where the relative grating roll angles were measured again with the SLRT. Details on experimental procedure and data analysis for PANTER x-ray testing can be found in Ref. 7. Figure 3 shows two pseudo-windows mounted to a pseudo-petal along with the used scanning paths for the alignment of four gratings (the petal had to be scanned twice due to limited travel range of the XY stage). First, two pairs of CAT gratings were aligned within two pseudo-windows (two gratings per window), one pair per each window, following the same procedure as described in our previous paper [23]. After aligning two gratings on each pseudo-window, window-level alignment was performed by adjusting the roll angle of the pseudo-window two using a micrometer and spring plunger (see Fig. 3) while scanning two adjacent gratings from each window (X14 and X13). The window-level alignment was repeated until all 6 pairs of relative roll angles between the four gratings satisfied the Arcus allocation of 5 arcmin [19, 20].

After the window-level alignment was performed, relative roll angles between the four gratings were measured by scanning across the pseudo-petal using the SLRT (it takes two scans, with the pseudo-petal shifted between scans due to the limited range of travel for the translation stage (see Fig. 3)). Then, all the facets and windows were carefully tacked with epoxy to prevent mechanical drift during travel between PANTER and MIT. Roll angle drift during the epoxy curing process is estimated to be negligibly small (less than metrology error). Figure 4a shows change of roll angles across the gratings after the alignment was completed. Data in green circles are noisier due to PSD centroid error induced by distortions of the reflected and diffracted beams from buckled membrane areas, and were neglected when averaging the relative roll angles (only regions shaded in red were averaged).

Table 1 summarizes the relative roll angles (referenced to X13) and metrology uncertainties for SLRT and x-ray measurements [7]. Roll angles measured with the two independent metrologies indicate that Arcus alignment allocations were satisfied for all six pairs of relative roll angles. However, roll angles for X10 and X15 don't agree between SLRT

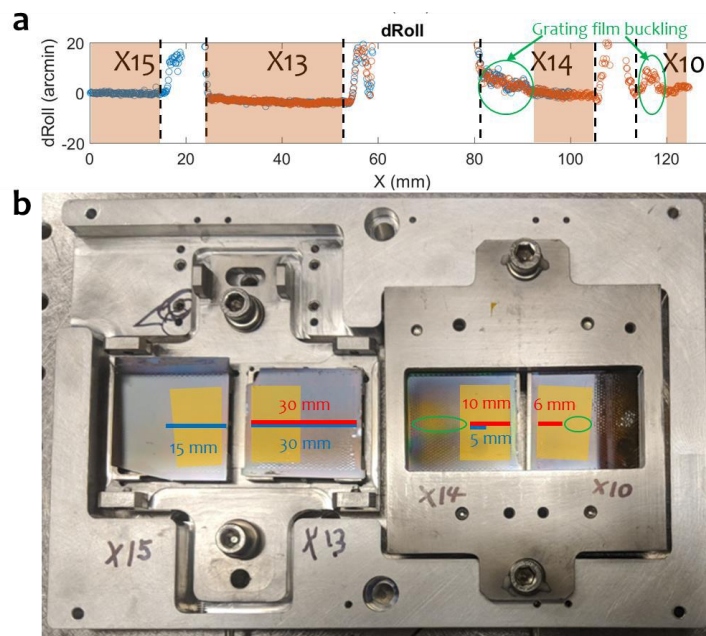


Figure 4. (a) Measured roll variations across four gratings. Red: a first scan from X10 to X13. Blue: a second scan from X14 to X15. (b) Photograph of a pseudo-petal with four gratings aligned and epoxied. Blue and red lines corresponds to the scanned path used to calculate relative roll angles for SLRT measurements. Green circles indicate regions found to have buckled grating films. Orange boxes indicate regions where gratings were illuminated with x rays using two confocal silicon pore optics (SPO) at PANTER.

and x-ray measurements. Since all hardware was epoxied to prevent mechanical drifts during travel, the difference could arise from metrology uncertainty. There are several possible explanations for discrepancies between the measurements. First, given a non-repeatable scanning path (scan path repeatability < 1 mm in the cross-dispersion direction) for the SLRT, it is possible that there had been an accumulation of PSD centroid error that depends on the precise scanning path. Second, the regions of the gratings scanned by SLRT or illuminated by x rays were different (see Fig. 4b). Third, change of surface heights induced by warpage of the gratings (even though the measured slopes varied less than 5 arcmin across the gratings in both dispersion and cross-dispersion axes) can cause a metrology error.

5. PINCHED GRATING BARS

Pinching of grating bars (two neighboring grating bars stick together, which can be observed with a scanning electron microscope, but has become rare in the latest generations of CAT gratings due to fabrication advances) makes the grating period to be effectively ~400 nm, possibly generating a so-called ‘half’ diffraction order between the zeroth and -1st diffraction order. A high gain photodetector (4.75×10^6 V/A) was placed at a diffraction angle of a half order (2.6 degree from surface normal). However, no discernable signal was detected even from an old low quality grating, putting into

Table 1. GWAT alignment results and metrology uncertainties. Different metrology uncertainties between gratings for SLRT are due to a stack of errors when being referenced to X13 from two subsequent scans. X13 was used as a reference to compare to other gratings.

	X10	X14	X13	X15	Note
Roll [arcmin]	2.7 ± 1.1	1.0 ± 0.7	0 (Ref.)	4.3 ± 0.9	SLRT measurement before PANTER
	-1.4 ± 1.4	1.6 ± 1.4	0 (Ref.)	-0.7 ± 1.4	PANTER x-ray measurement
	4.8 ± 1.1	3.1 ± 0.7	0 (Ref.)	3.4 ± 0.9	SLRT measurement after PANTER

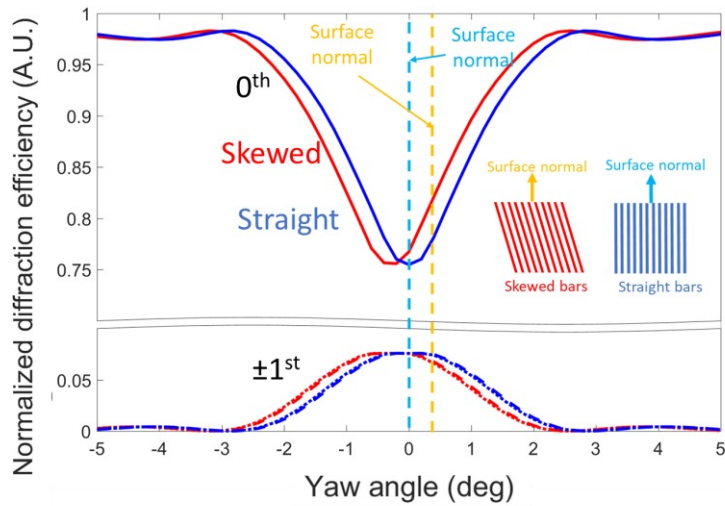


Figure 5. Simulated diffraction efficiencies for 0^{th} (solid), $+1^{\text{st}}$ (dotted), and -1^{st} orders (dashed) as a function of yaw angle relative to the surface normal for straight (blue) and skewed (red) bars. The orange and blue dotted lines indicate grating surface normals.

question the sensitivity of this method. We will attempt modeling of the expected UV diffraction efficiency from pinched lines to investigate this method further.

6. METROLOGY FOR GRATING BAR TILT ANGLES

The transmission of x rays through a CAT grating is strongly dependent on the angle of incidence relative to the grating bars and symmetric around the angle where x rays are parallel to the grating bars (assuming a rectangular grating bar profile, for example). We used a commercial SAXS tool with a well-collimated, $50\ \mu\text{m}$ -diameter x-ray beam of $\text{Cu-K}\alpha$ radiation and a CCD camera 1.5 m downstream of the grating holder. The custom-designed grating holder sat on a goniometer stage that placed the grating surface and the x-ray beam in the center of the goniometer rotation. The grating was rotated around an axis in the surface of the grating and parallel to the grating bars (grating yaw rotation, see Fig. 6a, b). Diffraction efficiencies for 0^{th} and $\pm 1^{\text{st}}$ orders were simulated based on rigorous coupled-wave analysis (RCWA) to understand how diffraction efficiencies change as a function of yaw angle (see Fig. 5). Skewed and straight silicon grating

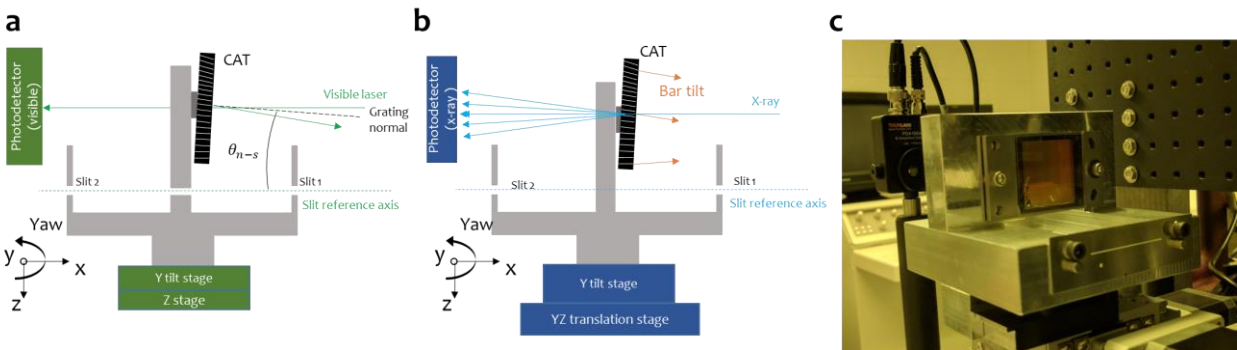


Figure 6. Schematic for the optical surface normal measurement (OSNM) setup (a) and SAXS setup (b) with custom grating holder. (c) A photograph of the custom grating holder mounted on the OSNM setup.

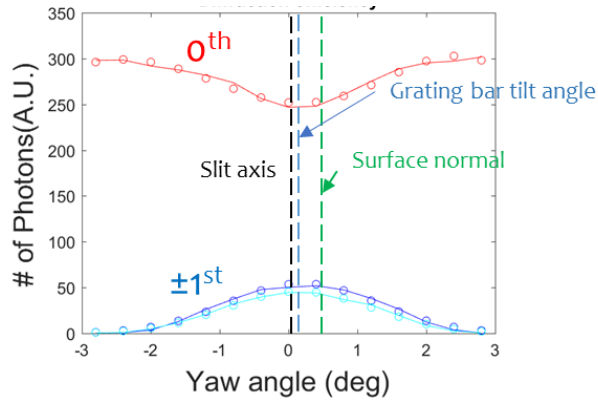


Figure 7. Measured photon counts for 0th and $\pm 1^{\text{st}}$ orders as a function of yaw angle from a single hexagonal grating film. Slit axis, surface normal, and grating bar tilt angles are all shown.

bars with 200 nm pitch, 30% duty cycle, and 4- μm thickness were modeled and compared. Surface normals for both skewed and straight bars were modeled to be located at a ‘zero’ yaw angle. The minimum (or maximum) of the 0th (or 1st) orders indicate the angle where the x rays are incident parallel to the grating bars, which we call ‘bar tilt angle’. The simulation results show no discernible difference except that the bar tilt angle for a grating with skewed bars is located at a ‘non-zero’ yaw angle. This clearly indicates that the SAXS tool is not sensitive to the angle of the surface normal relative to the x-ray beam, but it can be used to measure changes in grating bar tilt angles across a grating if the grating can be scanned across the stationary x-ray beam.

A measurement protocol to find bar tilt angles relative to the grating surface normal was developed based on two independent setups – SAXS and optical surface normal measurement (OSNM) tools (see Fig. 6a, b). A custom grating holder with integrated slits was designed (see Fig. 6c). The slit axis was used as a reference artifact to relate angles measured from OSNM and SAXS setups. First, a grating holder was placed on the OSNM setup to measure the relative angle between the grating surface normal and the slit axis (θ_{n-s}). Next, the mount was moved to the SAXS setup where the angles between grating bars and the slit were measured. After SAXS measurement, the mount was placed back on the OSNM setup to measure the slit-to-surface normal angle (θ_{n-s}) again.

The OSNM was built using a green HeNe laser, a photodetector, a high-precision vertical stage (12 arcsec of yaw error), and tilt stage (Fig. 6a). After the custom grating holder was mounted on the OSNM setup, the slit reference axis

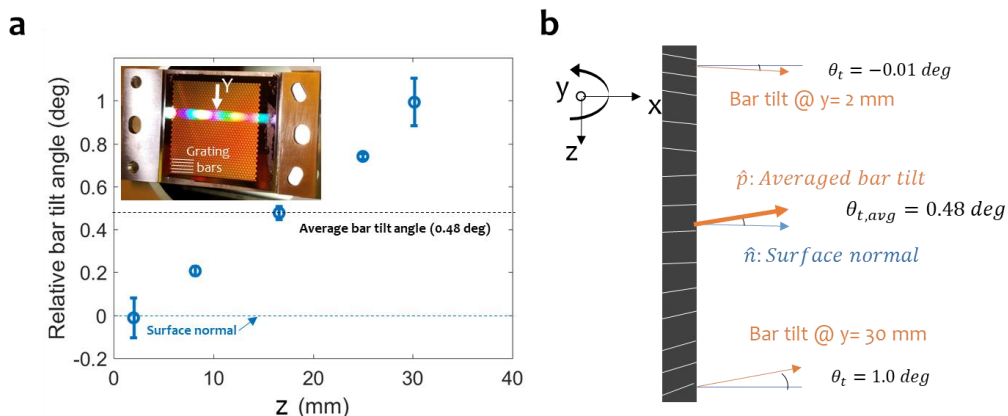


Figure 8. (a) Measured grating bar tilt angle variations along the dispersion direction for X14. Each data point averages 5 measurements at the same z but different values of y . Error bar indicates 1σ . (b) Visualization of grating bar tilt angle variations for X14.

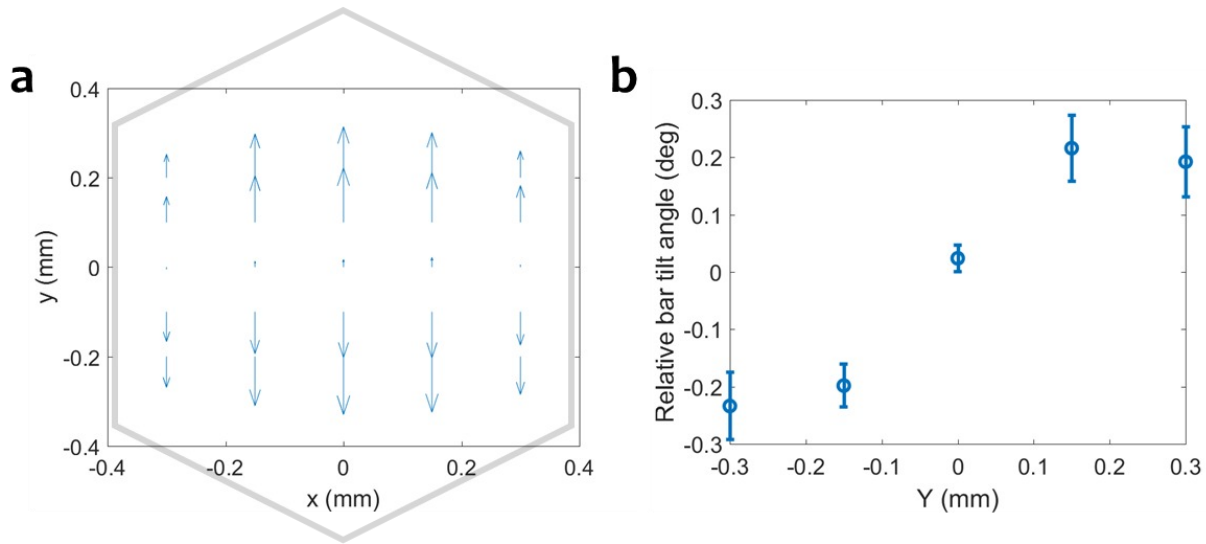


Figure 9. Measured bar tilt angle variations within a single hexagon located close to center of grating X10. (a) A quiver plot showing bar tilt angle variations as a function of position. (b) Relative bar tilt angle as a function of y within a single hexagon.

was aligned with the green laser by finding a yaw angle and Z position that allow maximum intensity for the laser passing through the slits. After finding the slit axis, the grating holder was translated vertically such that the beam is incident on the grating surface, and the slit-to-surface normal angle (θ_{n-s}) was found (Fig. 6b). The grating was scanned vertically to observe any potential warpage, which was measured to be ~ 0.1 degree. Next, the grating holder was moved into the SAXS setup where the slit axis was aligned with the x-ray beam following a similar process as described before. Then, the grating was scanned along y and z axes with $100 \mu\text{m}$ steps while measuring 0^{th} order intensity to find the center coordinate of each hexagonal grating film. A total of 25 coordinates were used (5 points along the z axis with 5 y values for each z position). At each of the coordinates, a SAXS measurement was performed to measure bar tilt angle relative to surface normal. The grating was yawed from -2.8 to 2.8 degree with 0.4 degree steps while counting the number of photons for 0^{th} and 1^{st} orders for 0.3 seconds to calculate relative diffraction efficiencies as a function of the yaw angle. The 0^{th} and 1^{st} order diffraction efficiencies were then fitted to Lorentzian profiles, and the angles at which the peaks were located were averaged to deduce bar tilt angles for each membrane. Lastly, the grating holder was moved back to the OSNM tool to measure the slit-to-surface normal angle (θ_{n-s}) again.

Figure 7 shows representative data for surface normal, slit reference axis, and grating bar tilt angle at a certain position on a grating. Figure 8 shows the distribution of bar tilt angle along the dispersion axis (y) and average bar tilt angles relative to surface normal for X14. Larger error bars are often associated with more buckled hexagon films in that row (see Fig. 8). This is due to the uncertainty in finding coordinates for centers of grating film. Figure 8b visualizes the data shown in Figure 8a. The grating bars were found to “lean” towards each other on the device layer surface, which is in line with the results from Refs. 27 and 28. This suggests that a non-uniform plasma sheath during DRIE has caused a systematic variation in bar tilt angle.

Table 2. Summary of measured grating bar tilt angles for several CAT grating samples.

Sample Name	X14	X10	X16	X17	X19	X21	X22	Average
Size	32 mm \times 32 mm			26 mm \times 27 mm				N/A
Average bar tilt angle [deg]	0.48 (10)	0.64 (10)	0.33 (10)	0.20 (10)	0.17 (10)	0.27 (10)	0.3 (10)	0.30
Total bar tilt angle variation [deg]	1.00 (13)	1.36 (32)	1.52 (47)	0.85 (89)	1.20 (30)	0.85 (5)	0.74 (24)	1.07
Rate of change of bar tilt angle along z [deg/mm]	0.036 (4)	0.044 (38)	0.054 (24)	0.046 (56)	0.055 (6)	0.047 (9)	0.038 (39)	0.046

Figure 9a shows a distribution of bar tilt angles within a single, strongly buckled grating film in X10. The same SAXS measurements as described above were performed at 25 points within the hexagon with steps of 150 and 100 μm along y and z axes. A grey hexagon is schematically drawn 'to scale'. Total bar tilt angle variation of ~ 0.45 degree was observed (see Fig. 9b) within this single hexagon. Since only 0.03 degree of bar tilt variation is expected for a 0.6 mm span from the measured long range variation (see Table 2), most of the ~ 0.45 degree of bar tilt angle variation is probably due to grating film buckling.

Table 2 summarizes average bar tilt angle relative to surface normal, total bar tilt angle variations, and rate of change of bar tilt angle for seven different CAT gratings. Average bar tilt angle and total bar tilt angle variations were found to be ~ 0.3 and ~ 1.0 degree, respectively. The average rate of change of bar tilt angle is found to be ~ 0.05 deg/mm. The measurement uncertainty for the average bar tilt angle is estimated to be 0.1 degree, mostly dominated by uncertainty in finding the slit reference axis in the OSNM setup. Very large differences for total bar tilt angle variation for different samples indicate that metrology is dependent on the quality of the CAT grating. Buckling of the grating film is thought to be a main contributing factor to sample-dependent metrology uncertainty. X14, X10, and X16 are large 32×32 mm gratings of which X14 and X10 were used for GWAT, and X17, X19, X21, and X22 are 26×27 mm size gratings planned to be used for a Flight-Like Alignment Test (FLAT) [7]. The values written in the Table follow the orientation shown in Fig. 8.

7. SUMMARY AND FUTURE WORK

The SLRT and SAXS metrology tools were developed for measurement of several potential grating imperfections. The SLRT was successfully used for GWAT, aligning four CAT gratings to satisfy Arcus roll alignment allocations (5 arcmin). However, non-repeatable scanning paths for the SLRT before and after x-ray test is estimated to degrade measurement repeatability. Three dowel pins could be used for repeatable mounting of the GWAT petal in the SLRT to improve repeatability. The SLRT is now being modified to form a grating facet alignment station (GFAS) by integrating a system that bonds gratings to the flight-like grating facet frames for the FLAT [7]. Alignment and bonding will both be performed with the GFAS for the FLAT.

The SLRT needs further improvement for period mapping and characterization of grating film buckling. Since buckling makes metrology more challenging, we are working on process improvements in grating fabrication along with metrology.

The SAXS and OSNM setups were used to characterize bar tilt angles for several CAT gratings. The fact that the grating bars were measured to "lean" towards each other on the device layer agrees well with Refs. 27 and 28. Our DRIE tool is a used, previous generation DRIE tool. In the future we plan to use a state-of-the-art DRIE tool which has demonstrated much reduced etch angle variations [27, 28] to decrease bar tilt angle variations.

Metrology precision needs to be improved by introducing a centroiding algorithm when finding the center of a grating film to reduce uncertainty propagated from buckled grating films. Beam size and slit width of the OSNM setup have to be optimized to reduce uncertainty in finding the slit reference axis. Furthermore, we are planning to do a more thorough analysis on the angle-dependent diffraction efficiency from the SAXS measurements to extract information about grating bar duty cycle and grating depth variations across gratings [29-31].

ACKNOWLEDGEMENTS

This work was supported by NASA grant NNX17AG43G. This work made use of the Shared Experimental Facilities supported in part by the MRSEC Program of the National Science Foundation under award number DMR – 1419807.

REFERENCES

- [1] Smith, R. K. *et al.*, “Arcus: the x-ray grating spectrometer explorer,” *Proc. SPIE* **10397**, 41 (2017).
- [2] Ptak, A. F. *et al.*, “Arcus: the x-ray grating spectrometer explorer,” *Proc. SPIE* **10699**, 77 (2018).
- [3] Collon, M. J. *et al.*, “Development of Athena mirror modules,” *Proc. SPIE* **10399**, 103990C (2017).
- [4] Heilmann, R. K., Bruccoleri, A. R., and Schattenburg, M.L., “High-efficiency blazed transmission gratings for high-resolution soft x-ray spectroscopy,” *Proc. SPIE* **9603**, 960314-1 (2015).
- [5] Heilmann, R. K. *et al.*, “Critical-Angle X-ray Transmission Grating Spectrometer with Extended Bandpass and Resolving Power > 10,000,” *Proc. SPIE* **9905**, 99051X-1 (2016).
- [6] Heilmann, R. K. *et al.*, “Critical-angle transmission grating technology development for high resolving power soft x-ray spectrometers on Arcus and Lynx,” *Proc. SPIE* **10399**, 1039914 (2017).
- [7] Heilmann, R. K. *et al.*, “Blazed transmission grating technology development for the Arcus x-ray spectrometer explorer,” *Proc. SPIE* **10699** (paper 228), to be published (2018).
- [8] Schattenburg, M. L. *et al.*, “Fabrication of high energy x-ray transmission gratings for AXAF”, *Proc. SPIE* **2280**, 17 (1994).
- [9] Ahn, M., Heilmann, R. K., and Schattenburg, M. L., “Fabrication of ultrahigh aspect ratio freestanding gratings on silicon-on-insulator wafers,” *J. Vac. Sci. Technol. B* **25**, 2593 (2007).
- [10] Ahn, M. Heilmann, R. K., and Schattenburg, M. L., “Fabrication of 200 nm-period blazed transmission gratings on silicon-on-insulator wafers,” *J. Vac. Sci. Technol. B* **26**, 2179-2182 (2008).
- [11] Mukherjee, P. *et al.*, “Plasma etch fabrication of 60:1 aspect ratio silicon nanogratings with 200 nm pitch,” *J. Vac. Sci. Technol. B* **28**, C6P70 (2010).
- [12] Heilmann, R. K. *et al.*, “Fabrication update on critical-angle transmission gratings for soft x-ray grating spectrometers,” *Proc. SPIE* **8147**, 81471L-1 (2011).
- [13] Bruccoleri, A. *et al.*, “Fabrication of nanoscale, high throughput, high aspect ratio freestanding gratings,” *J. Vac. Sci. Technol. B* **30**, 06FF03 (2012).
- [14] Bruccoleri, A. *et al.*, “Nanofabrication Advances for High Efficiency Critical-Angle Transmission Gratings,” *Proc. SPIE* **8861**, 886119 (2013).
- [15] Bruccoleri, A., Heilmann, R. K., and Schattenburg, M. L., “Fabrication process for 200 nm-pitch polished freestanding ultrahigh aspect ratio gratings,” *J. Vac. Sci. Technol. B* **34**, 06KD02 (2016).
- [16] Thomson, W., “Popular lectures and addresses, Electrical units of measurement, **1**, 73 (1883).
- [17] Dewey, D., Humphries, D. N., McLean, G. Y., Moschella, D. A., “Laboratory Calibration of X-Ray Transmission Diffraction Gratings,” *Proc. SPIE* **2280**, pp. 257-271 (1994).
- [18] Canizares, C. R., *et al.*, “The Chandra high-energy transmission grating: design, fabrication, ground calibration, and 5 years of flight,” *PASP*, **117**, 836, pp. 1144-1171 (2005).
- [19] Günther, H. M. *et al.*, “Performance of a double tilted-Rowland-spectrometer on ARCUS,” *Proc. SPIE* **10397** (26), (2017).
- [20] Günther, H. M. *et al.*, “Ray-tracing Arcus in phase A,” *Proc. SPIE* **10699** (230), (2018).
- [21] Anderson, E. H. Levine, A. M., Schattenburg, M. L., “Transmission x-ray diffraction grating alignment using a photoelastic modulator,” *Appl. Opt.* **27**, 16 (1988).

- [22] Fischbach, K. F. *et al.*, “Performance of high spatial frequency x-ray transmission gratings,” *Proc. SPIE* **982**, 31 (1988).
- [23] Song, J. *et al.*, “Scanning laser reflection tool for alignment and period measurement of critical-angle transmission gratings,” *Proc. SPIE* **10399**, 1039915 (2017).
- [24] Born, M. and Wolf, E. *Principles of Optics* (Cambridge University Press, 7th ed.), Chapter 8, 11.
- [25] Ferrera, J., Schattenburg, M. L., Smith, H. I., “Analysis of distortion in interference lithography,” *J. Vac. Sci. Technol. B* **14**, 4009 (1996).
- [26] Walsh, M. E., Ph.D. Thesis, Massachusetts Institute of Technology, “On the design of lithographic interferometers and their application,” (2004).
- [27] Barnett, R. *et al.*, “A new plasma source for next generation MEMS deep Si etching: minimal tilt, improved profile uniformity and higher etch rates,” *ECTC*, pp. 1056 – 1059 (2010).
- [28] Lea, L. and Nicholls, G. “Issues involved in etching Through Silicon Vias at high rate for reliable interconnects,” a report, Surface Technology Systems.
- [29] Hu, T. *et al.*, “Small angle x-ray scattering metrology for sidewall angle and cross section of nanometer scale line gratings,” *J. Appl. Phys.* **96**, 1983 (2004).
- [30] Sunday, D. F., List, S., Chawla, J. S., and Kline, R. J., “Determining the shape and periodicity of nanostructures using small-angle x-ray scattering,” *J. Appl. Crystal.* **48**, 1355 (2015).
- [31] Wang, C. Jones, R. L., Lin, E. K., Wu, W. L., and Leu, J., “Small angle x-ray scattering measurements of lithographic patterns with sidewall roughness from vertical standing waves,” *Appl. Phys. Lett.* **90**, 193122 (2007).